

Evaporation from Sand and Loess Soils: An Experimental Approach

Dewen Huang^{1,2} · Jiansheng Chen^{1,2,3,4} ·
Lucheng Zhan^{1,2} · Tao Wang^{1,2} · Zhiguo Su⁴

Received: 18 June 2015 / Accepted: 17 May 2016 / Published online: 8 June 2016
© Springer Science+Business Media Dordrecht 2016

Abstract In arid and semiarid areas, low rainfall and high evaporation make groundwater the main source of soil water in the vadose zone. In order to understand the upward migration rate of soil water and the mechanisms of moisture migration in the vadose zone, evaporation experiments in sand and loess soils were conducted. The evaporation and imbibition of the soil columns were measured in order to analyze the upward migration rate of soil water. Hydrochemical and isotopic methods were applied to investigate the microscopic mechanisms of water movement in the vadose zone. The results show that soil columns with higher loess contents have higher imbibition and evaporation rates. Obvious evaporation occurs only after soil water has reached the surface layer of the soil column, and the evaporation rate is related to soil composition. Salt migrates in the same direction as that of water movement and accumulates after the evaporation of water. The greater the evaporation, the greater the salt accumulation. Only strong hydraulic connections between soil water support the diffusion of salt from areas of higher concentration to those of lower concentration. Before liquid water reaches the surface layer, there are two regions of unsaturated soil. In the lower column, soil water moves in the form of liquid water and hydraulic connections are strong. In the upper column, water vapor from the lower column diffuses in soil pore spaces, and some are absorbed or condensed in the soil.

Keywords Evaporation experiment · Soil column · Unsaturated soil · Moisture migration · Stable isotopes

✉ Jiansheng Chen
jschen@hhu.edu.cn

¹ Key Laboratory of Ministry of Education for Geomechanics and Embankment Engineering, Hohai University, Nanjing 210098, China

² Jiangsu Research Center for Geotechnical Engineering Technology, Hohai University, Nanjing 210098, China

³ College of Earth Science and Engineering, Hohai University, Nanjing 210098, China

⁴ State Key Laboratory of Hydrology-Water Resources and Hydraulic Engineering, Hohai University, Nanjing 210098, China

1 Introduction

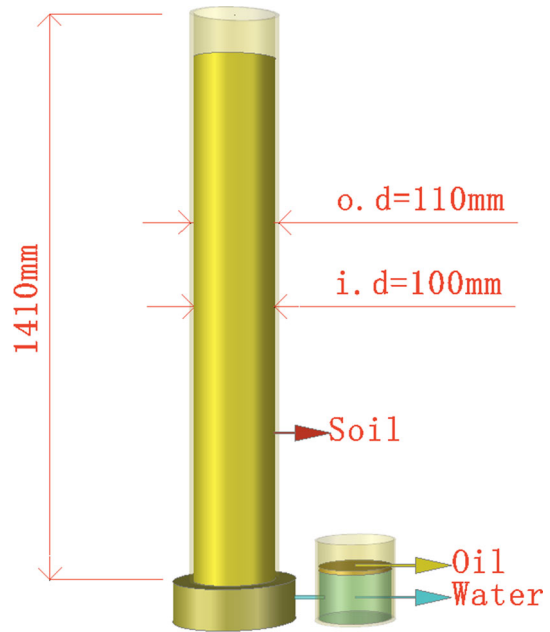
Low rainfall and high evaporation mean that groundwater is the main source of soil water in the vadose zone of arid and semiarid areas (Chen et al. 2004; Dong et al. 2016; Ma et al. 2014). The upward migration of groundwater through the unsaturated soil layer provides a valuable water resource for the growth of ground vegetation (Yang et al. 2014) and can also result in soil salinization. Improving our understanding regarding water movement mechanisms during the recharge process from groundwater to the unsaturated layer is of great significance for agriculture, land management, and ecological environment research in arid regions.

Moisture migration in unsaturated soils is significantly more complicated than that of saturated soils. The vapor–liquid–solid triphase system in soil pore spaces is complex due to the large number of variables and the complex configurations of the regions occupied by liquid and gas. Over the past decades, the theoretical research of the moisture migration in unsaturated soil had drawn great attention and much progress had been achieved (Haines 1925; Lebeau and Konrad 2010; Richards 1931). During the period 1902–1906, based on the theoretical and experimental research of soil physics, Buckingham firstly proposed a series of concepts as a distinct property of unsaturated soils, including matric potential, soil water retention curve, and unsaturated hydraulic conductivity (Nimmo and Landa 2005), and used an equation to quantify flow in unsaturated soil, a theory later known as Darcy–Buckingham law (Narasimhan 1998). His research formed part of the foundation of multiphase flow in porous media (Narasimhan 2005). In 1931, Richards introduced the equation of heat conduction in metals into the capillary water flow in porous media and derived the Richards equation (Miller and Miller 1956; Pachepsky et al. 2003; Richards 1965), which advanced the development of the theory of water movement in unsaturated soils (Weill et al. 2009; Zhou et al. 2013). According to the Richards equation, soil water transport in unsaturated soil hinges on the hydraulic conductivity and water retention. In many cases, however, it is difficult to measure the hydraulic conductivity by means of experiment (Lebeau and Konrad 2010). As an alternative to direct measurements, parametric models have been widely used to estimate hydraulic conductivity and water retention from data that are more easily obtained (Mohammadi and Vanclooster 2011; Mohammadi and Meskini-Vishkaee 2012; Yang et al. 2014). Lebeau and Konrad (2010) proposed a predicting model, which accounts for both capillary and thin film flow processes, to study the hydraulic conductivity of unsaturated soil. Nimmo (2010) combined source-responsive flow with diffuse flow and presented a theory for source-responsive and free-surface film modeling of unsaturated flow, which prompted a discussion on the theory of unsaturated flow (Germann 2010; Masciopinto 2012; Nimmo 2010, 2012).

Many studies have also been devoted to the experiment of soil water movement in unsaturated soils (Ewing 2004, 2006; Hirasaki 1991; Kawamoto et al. 2004). Changes in water content or matric suction in unsaturated soils were used in traditional experiments to investigate the mechanisms of soil water movement (Richards et al. 1957). The stable isotopic method was introduced to the experimental research of soil water movement in unsaturated soils (Allison and Barnes 1983a, b; Allison et al. 1983). Since then, a numerous studies based on the isotopic method sprung up in the literatures (Chen et al. 2012a, b; Liu et al. 1995; Shurbaji and Phillips 1995). The application of this new technology further promoted the development of the studies into unsaturated soil moisture migration.

The objective of this study was to investigate the mechanisms of soil water movement during groundwater upward migration. Experimental research of a long-term duration was presented in this paper. The effects of soil composition on rates of water movement were

Fig. 1 Schematic diagram of soil column apparatus



analyzed using parallel experiments with different soil compositions. The imbibition and evaporation of soil columns were measured in order to investigate soil water migration rates. Finally, stable isotopic and hydrochemical methods were used to investigate micromechanisms of soil water and salinity movement during groundwater upward migration.

2 Materials and Methods

2.1 Experimental Apparatus and Materials

The experimental apparatus consisted of a soil column and water container (Fig. 1). The column had an inner diameter of 100 mm and a length of 1410 mm. The inner diameter of the water container was the same as that of the soil column, but the length was 120 mm. Horizontal lines were carved on the water container at heights of 90 and 100 mm. The water container was connected to the soil column with a water hose, through which water in the water container flowed to the soil column. This simple design, which did not include electronic sensors, allowed for minimum interference and the simplest approach.

The compositions of soils used in the experiments were prepared according to the soil compositions of arid and semiarid areas, which are characterized by various ratios of sand and loess. Sand and loess were both processed using a drying treatment before mixing. The grain size distribution of sand is shown in Fig. 2, and the grain sizes of loess particles were mostly <0.075 mm.

2.2 Experimental Design

Three soil column experiments were conducted in parallel (Table 1) and mainly included three stages: the filling of soil columns, the measurements of the imbibition and evaporation, and

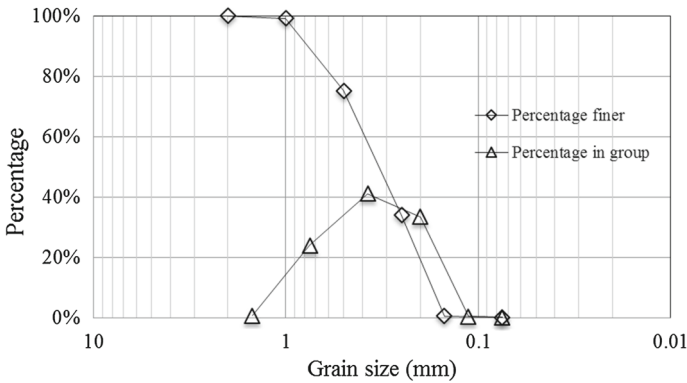


Fig. 2 Grain size distribution of sand

Table 1 Details of three soil columns

No.	Mass ratio between loess and sand	Height of column (mm)	Height of soil in column (mm)	Loading density (g/cm ³)	Mass percent of loess (%)
1	0:1	1410	1200	1.57	
2	1:2	1410	1200	1.62	33
3	1:1	1410	1200	1.61	50

the sampling and testing of soil columns. The measurement of the imbibition and evaporation was the longest stage, lasting for 348 days (October 2013–September 2014).

First, 6- to 8-mm gravel was loaded at the bottom of each soil column to a depth of 10 cm in order to simulate a saturated aquifer below the groundwater table. The sand/loess mixture was then loaded above the gravel to a total mixture soil column height of 1.2 m. The soil mixture and gravel layer were separated by a filter screen, which prevented the upper soil mixture from falling into the lower gravel layer. To ensure the uniformity of the filling soil density, soil was filled in layers, each of 10 cm in thickness.

After soil filling, the water container was connected to the soil column and then water was recharged to the upper carved horizontal line. Frequent water recharge ensured a relatively stable water level in the water container. Each water recharge time and the volume of recharged water were recorded in order to calculate the imbibition rate. Oil was used to cover the water in the water container to prevent evaporation from the water surface. Furthermore, each water container was covered by a 10 × 10 cm Perspex sheet to prevent interference from dust in the air. In order to avoid differences in the salinity and isotopic composition of recharge water, 500 l of water was stored in a big plastic kettle that was stored in a shaded area to avoid light contamination.

2.3 Measurement Methods

The temperature and relative humidity in the laboratory were monitored using a WSB-2 electronic hygrothermograph. The accuracy and precision of the measured temperature were ±1 and 0.1 °C, respectively. The accuracy and precision of the measured relative humidity were ±5 and ±1 %, respectively. Indoor temperature and relative humidity were monitored

last from October 20, 2013, to November 8, 2014. The highest and lowest temperatures, and the maximum and minimum relative humidity were recorded at each time interval.

In order to investigate the inhibiting effect of oil cover on water surface evaporation under laboratory conditions, two water evaporation experiments, one with oil cover and one without, were conducted in parallel with the soil column experiments. The apparatus of water evaporation experiment was the same size as the water containers in the soil column experiments. By measuring the mass changes of the two water containers over time, the water surface evaporation rates were calculated and reported in millimeters per day (mm/day).

The imbibition rate was considered to be the rate of water migration from the water container to the unsaturated soil in the soil column. During the soil column experiments, water was recharged to the water containers to the level of the upper horizontal line. Thus, the amount of water recharged equaled the imbibition amount between the adjacent water recharge operations. Therefore, the average imbibition rate was calculated by dividing the amount of water by the time interval between two water recharge operations. Imbibition rates were reported as millimeter per day (mm/day).

During soil column experiments, soil water migrated from the bottom to the upper part of the soil column and the soil surface in the upper soil column represented the only soil water evaporation. To obtain data on evaporation, the combined mass of the soil column and water container was measured monthly (10 months from November 2013 to September 2014). The evaporation of the soil column was calculated according to Eq. (1):

$$E = M_f + M_w - M_l \quad (1)$$

where E is the evaporation between two weightings, M_f is the mass of the former weighting, M_l is the mass of the later weighting, and M_w is the amount of water recharged to the water container between two weightings.

An electronic scale with measuring range of 0–30,000 g and a precision of 1 g was used to weigh the soil column and water container. The accuracy of the electronic scale was affected by ambient temperature; however, the weighting had to be carried out under different temperatures in different seasons because of the long duration of the soil column experiments. As high accuracy was needed for the calculation of evaporation, a correction method was employed, in which standard weights were used as substitute for the soil column and water container. First, the soil column and water container were weighed on the electronic scale (reading is A). Second, the standard weights were substituted for the soil column and water container until the same reading was achieved. Thus, the total mass of the weights was the real combined mass of the soil column and water container. The mass of the standard weights did not change under different temperatures; therefore, temperature-related errors were not introduced by the correction method.

At the end of the experiment, soils samples were collected from the soil columns, and the distribution of soil water content, soil salinity, and the compositions of ^{18}O and deuterium (D) in the soil water were analyzed. The columns were sampled at intervals of 10 cm, totaling 12 soil samples for each soil column. Soil samples were stored in hermetic bags to prevent soil water evaporation.

Soil water content was analyzed using the oven-drying method, whose analytical precision is better than 1 %. For the analysis of soil salinity, soil samples were air-dried for 48 h, and then 20 g of air-dried soil was mixed with 100 ml of deionized water. The mixture was kept for 48 h and periodically stirred to ensure that all salts were completely dissolved. Next, the supernatant was filtered with filter paper for the measurement of total dissolved solids (TDS).

Soil salinity was calculated using Eq. (2):

$$SS = \frac{TDS_{su} \times V_{de}}{m_s} \quad (2)$$

where SS is soil salinity, TDS_{su} is the TDS values of supernatant, V_{de} is the volume of deionized water, and m_s is the mass of air-dried soil.

The TDS values of soil water at different depths were calculated using Eq. (3):

$$TDS_s = \frac{TDS_{su} \times V_{de}}{m_s \times w / \rho_w} \quad (3)$$

where TDS_s is the TDS values of soil water at different depths, TDS_{su} is the TDS values of supernatant, V_{de} is the volume of deionized water, m_s is the mass of air-dried soil, w is the water content of soil samples, and ρ_w is the density of water.

Soil water was obtained from soil samples using the vacuum distillation method (Shurbaji and Phillips 1995). The D and ^{18}O compositions of the soil water were analyzed using a MAT253 mass spectrometer at the State Key Laboratory of Hydrology-Water Resources and Hydraulic Engineering, Hohai University. The analytical precision of the MAT253 mass spectrometer was better than 0.1 ‰ for oxygen and 2 ‰ for hydrogen. The results were reported as per mil differences (δ) relative to standard values of V-smow,

$$\delta^{18}\text{O} \text{ or } \delta\text{D} = [(R_{\text{sample}} - R_{\text{smow}}) / R_{\text{smow}}] \times 1000 \quad (4)$$

where R is the ratio of D/H or $^{18}\text{O}/^{16}\text{O}$.

3 Results

3.1 Experimental Environment

The temperature and relative humidity in the laboratory during the experiments are shown in Fig. 3. Max T (maximum temperature) and Min T (minimum temperature), and Max RH (maximum relative humidity) and Min RH (minimum relative humidity) for each time interval were recorded using the WSB-2 electronic hygrothermograph. The ranges of Max T and Min T were 13.5–34.5 and 3.0–27.4 °C, respectively. Seasonal variations in laboratory temperature were clearly observed (Fig. 3). Higher temperatures were observed in summer (June–August), and lower temperatures occurred in winter (December–February). The ranges of Max RH and Min RH were 42–90 and 22–76 %, respectively, and were relatively stable in autumn (August–October). The Max RH in this period (autumn) was above 80 %, and the Min RH was between ~50 and 60 %. Seasonal variations in relative humidity were not observed, and the values of the Max RH were above 50 % for most of the experiment.

During the water evaporation experiment, multiple water recharge operations were performed because significant evaporation occurred without the oil cover. This experiment lasted for 393 days (October 2013–November 2014; Fig. 4). The evaporation of water in the experiment with the oil cover was close to zero, but was relatively high when the oil cover was not used. Thus, the oil cover was an effective method of preventing water evaporation from the water container.

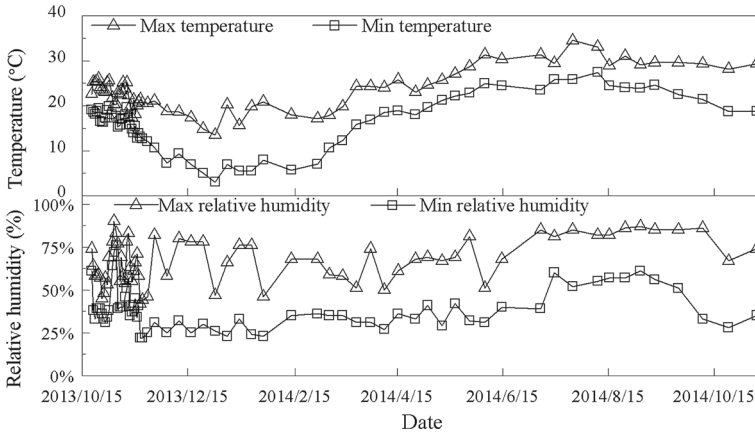


Fig. 3 Changes of temperature and relative humidity in laboratory over time

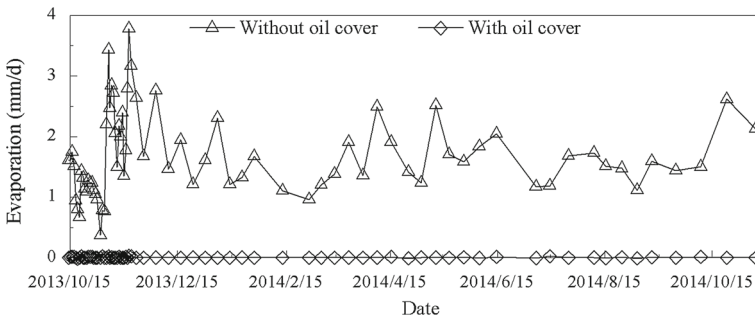


Fig. 4 Evaporation of water with and without oil cover

3.2 Imbibition and Evaporation

The imbibition rates of the three soil columns are shown in Fig. 5a. There was a decline in the imbibition rates during the first 3 months, followed by a relatively stable stage from March to June 2014. The imbibition rate of soil column 3 (Table 1) showed a small increase at the end of June 2014, and a fall during September 2014. However, the imbibition rate of soil column 1 did not show similar changes. The imbibition rate of soil column 3 was largest throughout the experiment, while that of soil column 1 was the smallest.

The evaporation rates of the three soil columns are shown in Fig. 5b. During the first 3 months of the experiment (December 2013–March 2014), the evaporation rates of the three soil columns remained close to 0 mm/day, indicating that water recharged from the water container had not reached the soil surface. After March 2014, the evaporation rate of soil column 3 increased significantly, reaching a maximum value (0.5 mm/day) in June 2014. There was a fall in the evaporation rate of soil column 3 during September 2014. The significant evaporation from column 3 between June and August indicated that soil water had moved to the soil surface allowing for steady evaporation. The fall in the evaporation rate may have been caused by temperature drops and the high relative humidity in the laboratory. The evaporation from soil column 2 remained close to 0 mm/day until April 2014, before rising slowly to 0.1 mm/day at the end of September, while that of soil column 1 remained

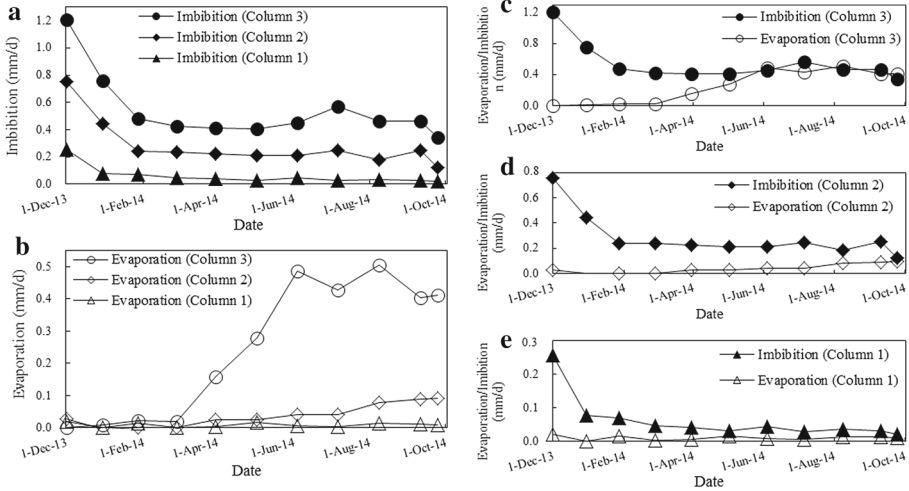


Fig. 5 Imbibition and evaporation rates of the three soil columns

close to 0 mm/day for the duration of the experiment. These results show that soil water in soil column 2 did not reach the column surface until April 2014, while that in column 1 never reached the soil surface.

A comparison of evaporation and imbibition for the three columns is shown in Fig. 5c–e. A dynamic equilibrium between the evaporation and imbibition rates was reached after June 2014. During the first 3 months of the experiment, no evaporation was observed in column 3; thus, imbibition water only became part of the soil water. After March 2014, the evaporation rate of column 3 increased. Therefore, the imbibition water was divided into two parts, with one becoming soil water and the other consumed by evaporation. The percentage consumed by evaporation increased with increasing column evaporation, and eventually the imbibition water was completely consumed by evaporation. Equilibrium between the evaporation and imbibition rates of column 2 was not reached until the end of September 2014. The fall of imbibition in this column at the end of September could be explained by the soil water reaching the maximum water-holding capacity and with evaporation the only reason for imbibition; however, the evaporation rate was smaller than the imbibition rate, and so, a fall in the imbibition rate was needed for it to equal the evaporation rate. The imbibition rate of column 1 after May 2014 was very small, while the evaporation rate was close to 0 mm/day throughout the experiment.

3.3 Water Content and Soil Salinity

The water content curves of the three soil columns are shown in Fig. 6. According to the differences in moisture content gradients, each water content curve was divided into three parts. The sections denoted in red represent moisture contents in regions closest to the simulated groundwater level. There were significant differences between the moisture content gradients in this region for the three columns, with the moisture content gradient of column 1 being 2.5 times that of column 2, and nearly 16 times of that of column 3. The moisture content gradients in the central parts of the columns are denoted in black and were similar for each column. The upper sections of the columns are denoted by hollow symbols. For column

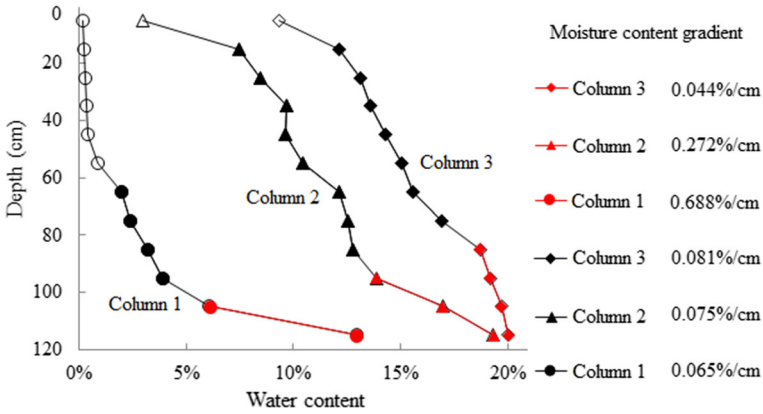


Fig. 6 Water content curves in three columns and the moisture content gradients in different part of the soil column

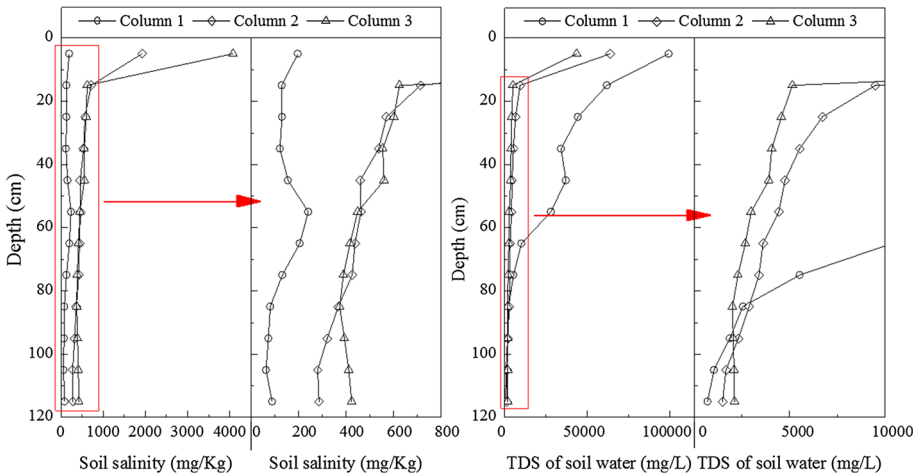


Fig. 7 Distributions of soil salinity and TDS values of soil water in three columns

1, this section was longer than the central section; however, and for the other two columns, the upper section denoted by the hollow symbols occupied only 10 cm.

The distributions of soil salinity in the three columns are shown in Fig. 7. The soil salinity at 5 cm depth in columns 2 and 3 was relatively high (1918 and 4073 mg/kg, respectively) before declining steeply to 713 and 624 mg/kg, respectively, at 15 cm depth. Below 15 cm, soil salinity decreased slowly with depth, reaching 286 and 423 mg/kg at 115 cm depth for columns 2 and 3, respectively. The high soil salinity observed in the upper layers of the soil columns implies that soil water moved in a liquid phase below 10 cm, as salts can only be carried to the surface by liquid soil water. Water in the surface layer was evaporated to the atmosphere; thus, leading to increased salinity in the surface layer. In the deeper layers, soil salinity was much lower reflecting the migration of salts from areas of high concentration to those of low concentration, a process that is ubiquitous in regions containing hydraulic connections. The soil salinity in column 1 peaked at a depth of 55 cm, and decreased with depth below 55 cm. There was a stable section in the soil salinity curve between 15 and 35 cm,

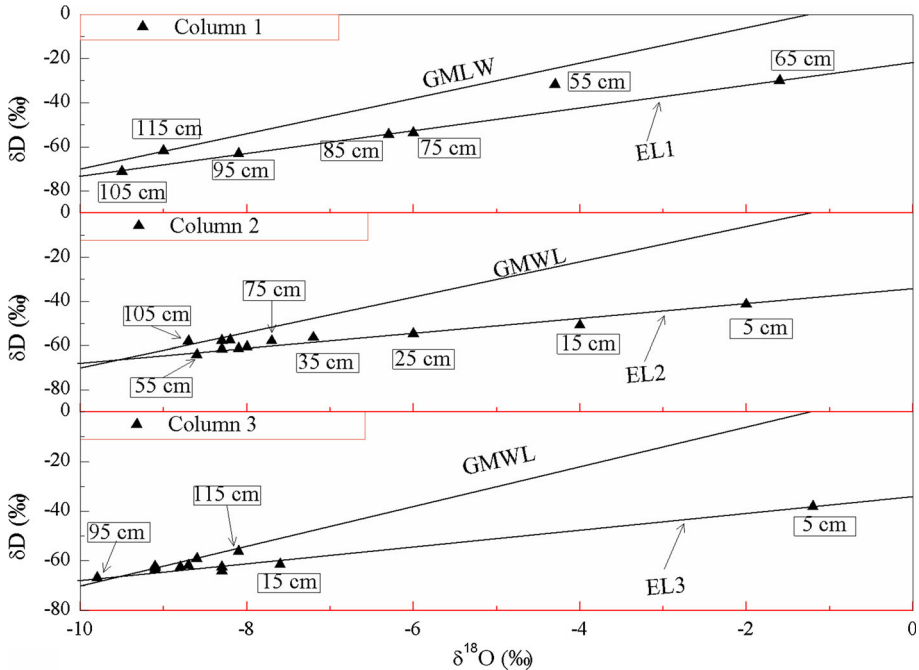


Fig. 8 Distributions of stable isotope data points of soil water in three columns: GMWL is the Global Meteoric Water Line, and EL is the Evaporation Line of soil water. The depths corresponding to the isotopic data points are marked beside them

which may not have been affected by the salinity carried by soil water. Soil salinity showed a slight increase at the soil surface, and this may have been caused by dust deposition from the air. The distribution of soil salinity in column 1 indicated that soil water did not reach the column surface and that the wetting front may only have reached a depth of 55 cm. The salt was carried to this region and formed slight salt accumulation.

The TDS values of soil water in the three columns are shown in Fig. 7b. The TDS values of soil water in column 1 were relatively small below 65 cm depth, and increased significantly above 65 cm. The TDS values of soil water between 15 and 85 cm depth in column 3 were smaller than those of soil water at the same depths in column 2. There may be because the relative larger moisture content in column 3 facilitated salt diffusion.

3.4 Soil Water Stable Isotope Compositions

The fractionation of stable isotopes during evaporation provides an effective method for studying soil water movement, and isotope compositions can reveal information on the evaporation intensity of soil water (Sun et al. 2009; Chen et al. 2012a, b). The stable isotope data for column 2 extended along a clearly defined evaporation line (EL2 in Fig. 8), with evaporation intensity decreasing with depth. At 35 cm depth and below, the soil water stable isotopes were very close to the Global Meteoric Water Line (GMWL), implying that little evaporation occurred in this region.

The soil water at 5 cm depth in column 3 was strongly influenced by evaporation, resulting in the enrichment of heavier isotopes. However, below 15 cm, the isotope compositions of soil water were close to the GMWL, indicating little evaporation.

In column 1, significant soil water was only observed at depths below 55 cm, and evaporation impacted water to depths of 65–85 cm. However, the isotope data for soil water at 55 cm depth implied that soil water at this depth mixed with condensed water formed from deeper sourced water vapor. This suggests that liquid water only reached a depth of ~65 cm, which is consistent with the distribution of soil salinity.

4 Discussion

There are different types of moisture migration in the unsaturated soil layer during groundwater upward movement. The results of the moisture content distributions in the three experimental columns indicated that there are three layers in the unsaturated zone above the simulated groundwater level. The layer closest to the simulated groundwater level (marked in red in Fig. 6) is characterized by capillary supporting water (Nia and Jessen 2015). Capillary force is the dominated driving force of soil water movement in this layer, and the soil water contents in this layer are very sensitive to the groundwater level. The heights of this layer and the moisture content gradients were different between the three columns. Column 3, which had the largest loess percent, had the widest capillary supporting layer. The layer above the capillary supporting layer (marked in black in Fig. 6) should be the film water layer. Soil water movement in this layer is mainly controlled by matric force, and hydraulic connections are strong. The layers close to the soil surface in columns 2 and 3 (marked as hollow symbols in Fig. 6) were influenced by evaporation. Poor hydraulic connections between soil water in this layer inhibited the diffusion of salt and heavy isotopes, which resulted in salt accumulation and heavy isotopes enrichment. The liquid soil water did not reach the soil surface in column 1; therefore, the upper layer (marked by hollow symbols) was little influenced by surface evaporation. Soil water in this layer was from deeper sourced water vapor. The decreased water content distribution was formed along the path of water vapor diffusion.

Soil composition is a factor affecting the migration rate of soil water. According to Fig. 5, the soil column with the highest loess percentage had the highest rate of soil water upward migration. It took 6 months (December 2013–June 2014) before equilibrium between evaporation and imbibition was reached in column 3, but in column 2 it was reached in 10 months (December 2013–October 2014). Liquid soil water never reached the soil surface in column 1.

5 Conclusions

In this study, we analyzed the upward migration rate of soil water in unsaturated soils and the mechanisms of soil water movement. Hydrochemical and isotopic methods were applied to the analysis and the following conclusions were made:

1. Soil with a higher loess percentage has a higher upward migration rate of soil water. Clear evaporation occurs only after soil water has reached the surface layer of the soil column, and the evaporation rate is related to soil composition.
2. Salt will migrate in the same direction as water movement, and accumulates after the evaporation of water. The greater the evaporation, the greater the level of salt accumula-

tion. Only good hydraulic connections between soil water facilitate the diffusion of salt from areas of higher concentration to those of lower concentration.

- Before liquid water reaches the surface layer, two regions exist in the unsaturated soil. In the lower part, soil water moves in the form of liquid water and hydraulic connections are strong. In the upper part, water vapor from the lower region diffuses into soil pore spaces and some is absorbed or condensed in the soil.

Acknowledgments The authors thank the State Key Laboratory of Hydrology-Water Resources and Hydraulic Engineering, Hohai University for sample analysis. The support of the National Basic Research Program of China (Grant No. 2012CB417005) and the Postgraduate Research and Innovation Plan Project of Jiangsu Province (Grant No. CXZZ12-0231) are gratefully acknowledged.

Compliance with Ethical Standards

Conflicts of interest The authors declare that they have no conflicts of interest.

References

- Allison, G.B., Barnes, C.J.: The distribution of deuterium and ^{18}O in dry soils: 1. Theory. *J. Hydrol.* **1–4**(60), 141–156 (1983a)
- Allison, G.B., Barnes, C.J.: Estimation of evaporation from non-vegetated surfaces using natural deuterium. *Nature* **301**, 143–145 (1983b)
- Allison, G.B., Barnes, C.J., Hughes, M.W.: The distribution of deuterium and ^{18}O in dry soils 2. Experimental. *J. Hydrol.* **64**(1), 377–397 (1983)
- Chen, J., Li, L., Wang, J., Barry, D.A., Sheng, X., Gu, W., Zhao, X., Chen, L.: Water resources: groundwater maintains dune landscape. *Nature* **432**(7016), 459–460 (2004)
- Chen, J., Sun, X., Gu, W., Tan, H., Rao, W., Dong, H., Liu, X., Su, Z.: Isotopic and hydrochemical data to restrict the origin of the groundwater in the Badain Jaran Desert, Northern China. *Geochem. Int.* **50**(5), 455–465 (2012a)
- Chen, J., Liu, X., Wang, C., Rao, W., Tan, H., Dong, H., Sun, X., Wang, Y., Su, Z.: Isotopic constraints on the origin of groundwater in the Ordos Basin of northern China. *Environ. Earth Sci.* **66**(2), 505–517 (2012b)
- Dong, C., Wang, N., Chen, J., Li, Z., Chen, H., Chen, L., Ma, N.: New observational and experimental evidence for the recharge mechanism of the lake group in the Alxa Desert, north-central China. *J. Arid Environ.* **124**, 48–61 (2016)
- Ewing, G.E.: Ambient thin film water on insulator surfaces. *Chem. Rev.* **106**(4), 1511–1526 (2006)
- Ewing, G.E.: Thin film water. *J. Phys. Chem. B* **108**(41), 15953–15961 (2004)
- Germann, P.: Comment on “Theory for source-responsive and free-surface film modeling of unsaturated flow”. *Vadose Zone J.* **9**(4), 1100–1101 (2010)
- Haines, W.B.: Studies in the physical properties of soils: II. A note on the cohesion developed by capillary forces in an ideal soil. *J. Agric. Sci.* **15**(04), 529–535 (1925)
- Hirasaki, G.J.: Wettability: fundamentals and surface forces. *SPE Form. Eval.* **6**(02), 217–226 (1991)
- Kawamoto, K., Mashino, S., Oda, M., Miyazaki, T.: Moisture structures of laterally expanding fingering flows in sandy soils. *Geoderma* **119**(3–4), 197–217 (2004)
- Lebeau, M., Konrad, J.M.: A new capillary and thin film flow model for predicting the hydraulic conductivity of unsaturated porous media. *Water Resour. Res.* **46**(12), W12554 (2010). doi:[10.1029/2010WR009092](https://doi.org/10.1029/2010WR009092)
- Liu, B., Phillips, F., Hoines, S., Campbell, A.R., Sharma, P.: Water movement in desert soil traced by hydrogen and oxygen isotopes, chloride, and chlorine-36, southern Arizona. *J. Hydrol.* **168**(1–4), 91–110 (1995)
- Ma, N., Wang, N., Zhao, L., Zhang, Z., Dong, C., Shen, S.: Observation of mega-dune evaporation after various rain events in the hinterland of Badain Jaran Desert, China. *Chin. Sci. Bull.* **59**(2), 162–170 (2014)
- Masciopinto, C.: Comments on “Theory for source-responsive and free-surface film modeling of unsaturated flow”. *Vadose Zone J.* **11**(4) (2012). doi:[10.2136/vzj2012.0015](https://doi.org/10.2136/vzj2012.0015)
- Miller, E.E., Miller, R.D.: Physical theory for capillary flow phenomena. *J. Appl. Phys.* **27**(4), 324–332 (1956)
- Mohammadi, M.H., Vanclooster, M.: Predicting the soil moisture characteristic curve from particle size distribution with a simple conceptual model. *Vadose Zone J.* **10**(2), 594–602 (2011)
- Mohammadi, M.H., Meskini-Vishkaee, F.: Predicting the film and lens water volume between soil particles using particle size distribution data. *J. Hydrol.* **475**, 403–414 (2012)

- Narasimhan, T.N.: Something to think about.. Darcy–Buckingham’s law. *Ground Water* **36**(2), 194–195 (1998)
- Narasimhan, T.N.: Buckingham, 1907. *Vadose Zone J.* **4**(2), 434 (2005)
- Nia, S.F., Jessen, K.: Theoretical analysis of capillary rise in porous media. *Transp. Porous Med.* **110**(1), 141–155 (2015)
- Nimmo, J.R.: Response to Germann’s “Comment on ‘Theory for source-responsive and free-surface film modeling of unsaturated flow’”. *Vadose Zone J.* **9**(4), 1102–1104 (2010)
- Nimmo, J.R., Landa, E.R.: The soil physics contributions of Edgar Buckingham. *Soil Sci. Soc. Am. J.* **69**(2), 328–342 (2005)
- Nimmo, J.R.: Response to “Comments on ‘Theory for source-responsive and free-surface film modeling of unsaturated flow’”. *Vadose Zone J.* **11**(4) (2012). doi:[10.2136/vzj2012.0044](https://doi.org/10.2136/vzj2012.0044)
- Pachepsky, Y., Timlin, D., Rawls, W.: Generalized Richards’ equation to simulate water transport in unsaturated soils. *J. Hydrol.* **272**(1–4), 3–13 (2003)
- Richards, L.A.: Capillary conduction of liquids through porous mediums. *J. Appl. Phys.* **1**(5), 318–333 (1931)
- Richards, L.A.: Physical condition of water in soil. In: *Methods of Soil Analysis. Part 1. Physical and Mineralogical Properties, Including Statistics of Measurement and Sampling*, pp. 128–152. Alliance of Crop, Soil, and Environmental Science Societies, Madison (1965)
- Richards, S., Weeks, L., et al.: Moisture movement in soils: experiments show moisture movement from one portion of soil to another and soil factors which influence that movement. *Calif. Agric.* **11**(4), 24–37 (1957)
- Shurbaji, A.M., Phillips, F.M.: A numerical model for the movement of H²O, H²¹⁸O, and ²HHO in the unsaturated zone. *J. Hydrol.* **171**(1), 125–142 (1995)
- Sun, X., Chen, J., Tan, H., Rao, W., Wang, Y., Liu, X., Su, Z.: Study on the mechanism of isotope fractionation in soil water during the evaporation process under equilibrium condition. *Chin. J. Geochem.* **28**(4), 351–357 (2009)
- Weill, S., Mouche, E., Patin, J.: A generalized Richards equation for surface/subsurface flow modelling. *J. Hydrol.* **366**(1–4), 9–20 (2009)
- Yang, H., Khoshghalb, A., Russell, A.R.: Fractal-based estimation of hydraulic conductivity from soil–water characteristic curves considering hysteresis. *Geotech. Lett.* **4**, 1–10 (2014)
- Zhou, J., Liu, F., He, J.: On Richards’ equation for water transport in unsaturated soils and porous fabrics. *Comput. Geotech.* **54**, 69–71 (2013)